Daniel Ramirez, Juliana Nanclares, Marisa Spontón, Mara Polo, Diana Estenoz and Franklin Jaramillo*

Effect of cooling induced crystallization upon the properties of segmented thermoplastic polyurethanes

DOI 10.1515/polyeng-2016-0106
Received March 18, 2016; accepted July 27, 2016

Abstract: An investigation on the cooling-induced crystallization in three thermoplastic polyurethanes based on MDI, PTMG, and 1.4-BD as chain extender with different hard segment content is reported. Thermal transitions were determined using differential scanning calorimetry (DSC) measurements at different cooling rates, and thermal stability was studied by thermogravimetric analysis. Changes in Raman spectra were useful to correlate the thermal transitions with changes in the morphology of the polymers. The dissimilarity in the composition gave different rheological behavior in the molten state, indicated by the temperature dependence of the viscosity. The mechanical properties and the crystallinity was influenced not only by the cooling rate but also by the hard segment content. Thermoplastic polyurethanes with more hard segment content formed more crystalline hard domains as evidenced by the DSC and atomic force microscopy results.

Keywords: cooling rate; crystallinity; mechanical properties; morphology; rheology.

1 Introduction

Polyurethanes (PURs) are very versatile materials [1]. Depending on the raw precursors, thermoplastic or thermoset PURs can be obtained. Thermoplastic PURs are linear segmented copolymers and have excellent mechanical properties and good biostability when they present high degree of crystallinity. It is important to note that the term crystallinity is a common term in the polymer community to indicate the amount of order and disorder in the polymer structure and does not refer to any crystal structure similar to that of a metal or an oxide material. This is the main reason for their wide range of applications in the field of adhesives, coatings, composites, and biomaterials [2–10]. PURs are usually composed of three monomers, a diisocyanate, a low molecular diol (also known as chain extender), and a macrodiol. The reaction between these monomers forms a segmented copolymer composed of hard and soft segments. The hard segments (HSs) are formed when the chain extender is added to the diisocyanate, and the soft segments (SSs) correspond to the macrodiol linked to the HS. The incompatibility between polar HSs and non-polar SSs leads to the formation of a two-phase microstructure. HSs can form carbonyl to amino-hydrogen bonds and thus tend to aggregate into ordered hard domains (HDs), whereas the SSs form amorphous or soft domains (SDs).

The properties of PURs are related to the degree of separation between SDs and HDs. The microphases separation has been studied by atomic force microscopy (AFM) [11], also as a function of the glass transition temperature (*Tg*) and the block lengths [12, 13]. Crawford et al. [14] synthesized different PURs, one of them based on poly(tetramethylene ether glycol) (PTMG), 1-isocyanato-4-[(4-isocyanatophenyl)methyl] benzene (MDI), and butane-1,4-diol (1,4-BD), and analyzed the morphology, the thermal properties, and the aging of the synthesized materials.

Lu et al. [15] studied the behavior of thermoplastic PURs obtained by extrusion and found that both rheological and thermal properties are very dependent on the thermal history. Yoon and Han [16] highlighted the importance of considering the processing of these materials, and therefore they focused only on the rheological behavior of PURs.

***Corresponding author: Franklin Jaramillo,** Centro de Investigación, Innovación y Desarrollo de Materiales-CIDEMAT, Universidad de Antioquia UdeA, Calle 70 No 52-21, Medellín, Colombia, e-mail: franklin.jaramillo@udea.edu.co
Daniel Ramirez and Juliana Nanclares: Centro de Investigación, Innovación y Desarrollo de Materiales-CIDEMAT, Universidad de Antioquia UdeA, Calle 70 No 52-21, Medellín, Colombia
Marisa Spontón, Mara Polo and Diana Estenoz: INTEC, Universidad Nacional del Litoral-CONICET, Güemes 3450, 3000 Santa Fe, Argentina

Hernandez et al. [17] synthesized a series of PURs based on PTMG, MDI and 1,4-BD, using different HS/SS composition, and analyzed the morphology by AFM, differential scanning calorimetry (DSC), and Fourier transform infrared spectroscopy. They observed discrete phases separation of the HS in the order of 10 nm. In order to achieve a more complete characterization of these systems, Castagna et al. [18] later studied the effect of the HS on the molecular dynamics by means of dielectric spectroscopy.

Despite the fact that many investigations on the thermal annealing behavior of these materials have been published, there is a lack of study on crystallization from the molten state related to the HD content, its effect on the morphology upon solidification, and the ultimate properties of the resultant product. In this study the morphology development of two PURs with different HS content is investigated using thermogravimetric analysis (TGA), DSC, Raman spectroscopy, and nanoindentation. Rheological behavior was also studied in order to correlate the HS content with the flow and viscoelastic properties in molten state.

2 Materials and methods

1-Isocyanato-4-[(4-isocyanatophenyl)methyl] benzene (isocyanate content ≈33% NCO), 1,4-BD as chain extender, and PTMG (number average molecular weight Mn ≈ 1000 g/mol, hydroxyl number = 107.0–118.0 mg KOH/g), were purchased from Sigma Aldrich (Saint Louis, MO, USA). Solvents were purchased from Mallinckrodt Chemicals (Saint Louis, MO, USA) and were distilled before use.

2.1 Synthesis of PURs

For the synthesis of the thermoplastic PURs a two-step solution polymerization was carried out. In order to remove the residual water before using, the PTMG was dried at 100°C under vacuum for 1 h in a 100 ml two-necked round-bottom flask equipped with a stirrer. Then, MDI dissolved in tetrahydrofuran was slowly added, and the reaction proceeded for 2 h under a dried nitrogen atmosphere at 60°C. Finally, 1,4-BD was also slowly added and allowed to react for 48 h. The polymer obtained was dissolved in dimethylformamide (DMF), precipitated on distilled water, and dried under vacuum for 2 weeks to allow the morphology to completely develop. The stoichiometry (molar ratio MDI:1,4-BD:PTMG) used for the samples was PUR1 = 1:0.5:0.5, PUR2 = 1:0.6:0.4, and PUR3 = 1:0.7:0.3.

2.2 Thermal analysis

Thermal stability was measured by thermogravimetric analysis (TGA equipment model 00 from TA Instruments) from room temperature to 650°C with a scan rate of 20°C/min under nitrogen atmosphere. DSC model 00 from TA Instruments was used to perform dynamic analysis in the range of 0°C–220°C at a scan rate of 10°C/min and modulated DSC analysis in order to measure the glass transition temperature with modulation amplitude of 0.159°C/min and modulation periods of 40 s.

2.3 Micro-Raman spectroscopy and nuclear magnetic resonance

Raman spectra of the samples were recorded using a Horiba Yvonjobin dispersive micro-Raman spectrophotometer equipped with a heating system for measurements at different temperatures under nitrogen atmosphere and using a 632.8 nm laser (He-Ne laser) for the excitation radiation. All the spectra were collected in the range 3700–100 cm^{-1}. A Bruker AMX-300 spectrometer was used to acquire the proton nuclear magnetic resonance spectra (^{1}H-NMR). Samples were dissolved in DMSO-d_6, and tetramethylsilane was used as internal standard. The experiments were carried out at 300 MHz.

2.4 Atomic force microscopy

Topography and phase images were taken in a VECCO Multimode Atomic Force Microscope. Amplitude modulation mode operating in the repulsive regime (phase <90°) with Cantilever was APPNano ACLA-20 radius <10 nm, spring constant k = 14.45 N/m, frequency f_0 = 175.6 kHz, free amplitude A_0 = 49.7 nm, and set point amplitude A_{sp} = 24.8 nm.

3 Results and discussion

3.1 Structural characterization

The structure of PURs synthesized was confirmed by ^{1}H-NMR spectroscopy (Figure 1). Both spectra of PUR1 and PUR3 present similar signal shifts. The signal at 9.48 ppm is associated with the proton of the amine group N-H; the signals corresponding to aromatic proton appear in the region between 7.33 and 7.05 ppm. Furthermore, the

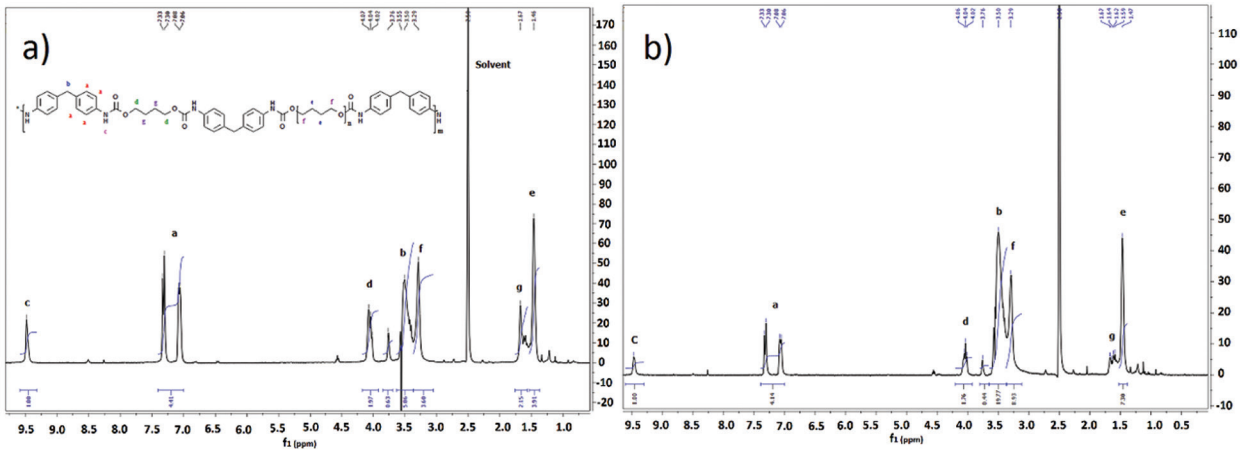

Figure 1: ^{1}H-NMR spectra of PUR3 (A) and PUR1 (B).

protons of $-COOCH_2$ groups show corresponding signals at 4.04 ppm; methylene groups of MDI appear at 3.50 ppm and the signals associated with $-OCH_2$ groups of PTMG at 3.29 ppm. Protons of internal saturated CH_2 from the PTMG are observed at 1.46 ppm, but aliphatic CH_2 signals derived from 1,4-butanediol were observed at 1.67 ppm.

Two main differences between PUR1 and PUR3 spectra were observed. The first one is the intensity ratio between e and g signals; PUR3 spectrum shows higher intensity of g peak corresponding to internal CH_2 due to the higher HS content. The second difference is the intensity ratio between signals assigned to -$COOCH_2$ groups of HS at 4.04 ppm and -OCH_2 groups of SS at 3.29 ppm. The calculated [HS]/[SS] intensity ratio was lower (0.2) for PUR1 than for PUR3 (0.5).

Dilute solution viscosities were determined in DMF at 25°C at four different concentrations, and plots of (ηsp/c) versus (c) for these samples were obtained. Some authors have used this method to have an idea of the relative molecular weight of PURs because sometimes it is not fully possible to use gel permeation chromatography [19]. From these plots the intrinsic viscosity [η] values were determined to be $[\eta]_{PUR1} = 0.21$ dl/g, $[\eta]_{PUR2} = 0.31$ dl/g, and $[\eta]_{PUR3} = 0.34$ dl/g. These intrinsic viscosity values indicate higher average molecular weight for PUR3.

3.2 Differential scanning measurements

DSC results for PURs are shown in Figure 2. In the cooling scan, PUR1 showed two endothermic peaks at 59.02°C and 116.79°C, which can be associated to both SS-HS interactions and crystallization of HDs [19]; as expected, during the heating cycle two endothermic peaks were also found; the first one could correspond to the phase separation transition involving weak micro-HSs aggregation, and the second could be attributed to the melting of microcrystalline HDs [20]. However, for PUR2 and PUR3 during the first cooling cycle, a defined exothermic peak can be seen at 179°C and 140°C, respectively, which is associated only to the HS crystallization. The thermal transition corresponding to the phase separation is indicated in the graph as red areas, while the melting of the HDs is indicated as purple.

The glass transition temperature was shown to be −59°C, −57°C, and −53°C for PUR1, PUR2, and PUR3, respectively. The higher Tg for PUR1 suggests that the HSs were not highly interacting to form microdomains. Also, it can be said that they were relatively freely dispersed in the SS, therefore requiring higher Tg (a scheme of the morphology is shown in Figure 5) [21], contrary to what happened with PUR2 and PUR3, in which higher content of HSs could form HDs giving higher phase separation and therefore lower Tg of the SSs. This is also supported by the first of the two peaks in the cooling and heating cycles for PUR1, which as mentioned before can be due to the SS-HS microphase separation after HS and SS interactions.

In order to have a better understanding of the crystallization for the obtained polymers, new DSC analyses were made at heating and cooling rates of 40°C/min, and the corresponding results are shown in Figure 2C and D. In comparison with Figure 2A during crystallization, PUR1 also showed two endothermic and exothermic peaks. However, significant changes are detected for PUR2 and PUR3 due to the increase of the cooling rate (which also showed two exothermic peaks like PUR1). At higher cooling rate, the crystallization degree decreases, and shifts of the crystallization peaks were observed. Also, a broadening in the endothermic transition can be seen.

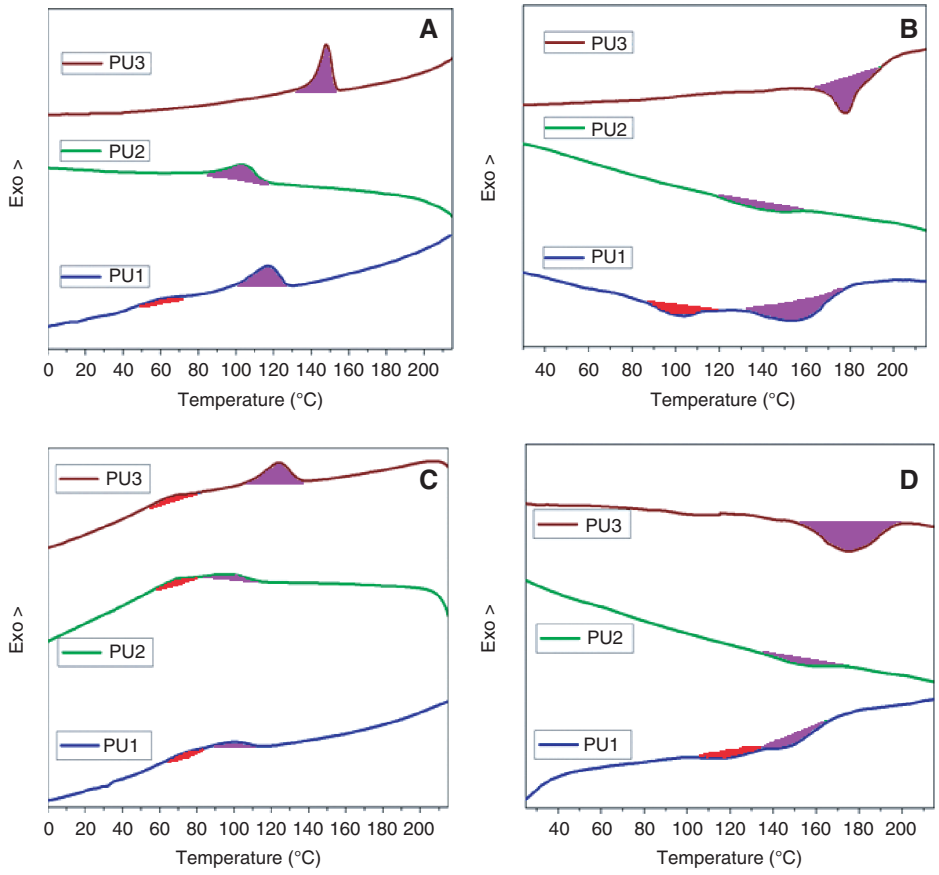

Figure 2: Thermograms obtained by DSC corresponding to (A) cooling and (B) heating at 10°C/min and (C) cooling and (D) heating at 40°C/min.

The results when cooling at 40°C/min indicated that even PUR2 and PUR3 with higher HS content can achieve HS-SS interactions, similar to those found by Nichetti and Grizzuti [22] when more crystalline PURs gave higher melting temperatures and broadening of the peaks. The rapid cooling does not allow a high crystalline arrangement of the HSs, because these HDs settle quickly, forming a heterogeneous distribution of HDs with a melting range of approximately 30°C (160–190°C). Finally, Table 1 summarizes the thermal properties obtained from DSC curves.

Table 1: Thermal properties of PURs.

Sample	T_c (°C)	ΔH_c (J/g)	T_f (°C)	ΔH_f (J/g)
10°C/min				
PUR1	59.02/116.79	1.35/5.19	101.94/156.91	1.15/4.21
PUR2	103.87	5.76	139.52	4.31
PUR3	157.85	21.10	193.75	19.34
40°C/min				
PUR1	77.13/99.91	1.13/4.87	109.50/137.23	1.12/1.37
PUR2	68.70/99.57	0.33/4.27	139.52	4.31
PUR3	66.16/124.02	3.27/12.11	178.58	9.18

3.3 Micro-Raman spectroscopy

In order to identify the structure change and as a complementary technique for the DSC measurements, Raman experiments For PUR1 and PUR3 were carried out at different temperatures, and then, when the final temperature (220°C) was reached, the samples were cooled at 10°C/min or 40°C/min.

Figure 3A shows the micro-Raman spectra for all samples. The positions of the characteristic bands of the functional groups remain the same in both samples. The characteristic vibration mode of C-O-C at 863 cm^{-1} was assigned to the aliphatic ether groups in the SSs. The bands for urethane amide, urethane amide II ($\delta NH + \nu(CN) + \nu(C-C)$), and urethane amide III ($\delta NH + \nu(CN)$) could be identified at 1534 cm^{-1}, 1182 cm^{-1}, and 1250 cm^{-1}, respectively [23]. The band at 1615 cm^{-1} was assigned to C=C of aromatic rings, the bands between 2800 and 3000 cm^{-1} correspond to symmetric and asymmetric C-H stretching vibrations of CH_2, and two weak peaks at 1698 cm^{-1} and 3225 cm^{-1} are related to the N-H stretching vibrations in hydrogen bond between nitrogen

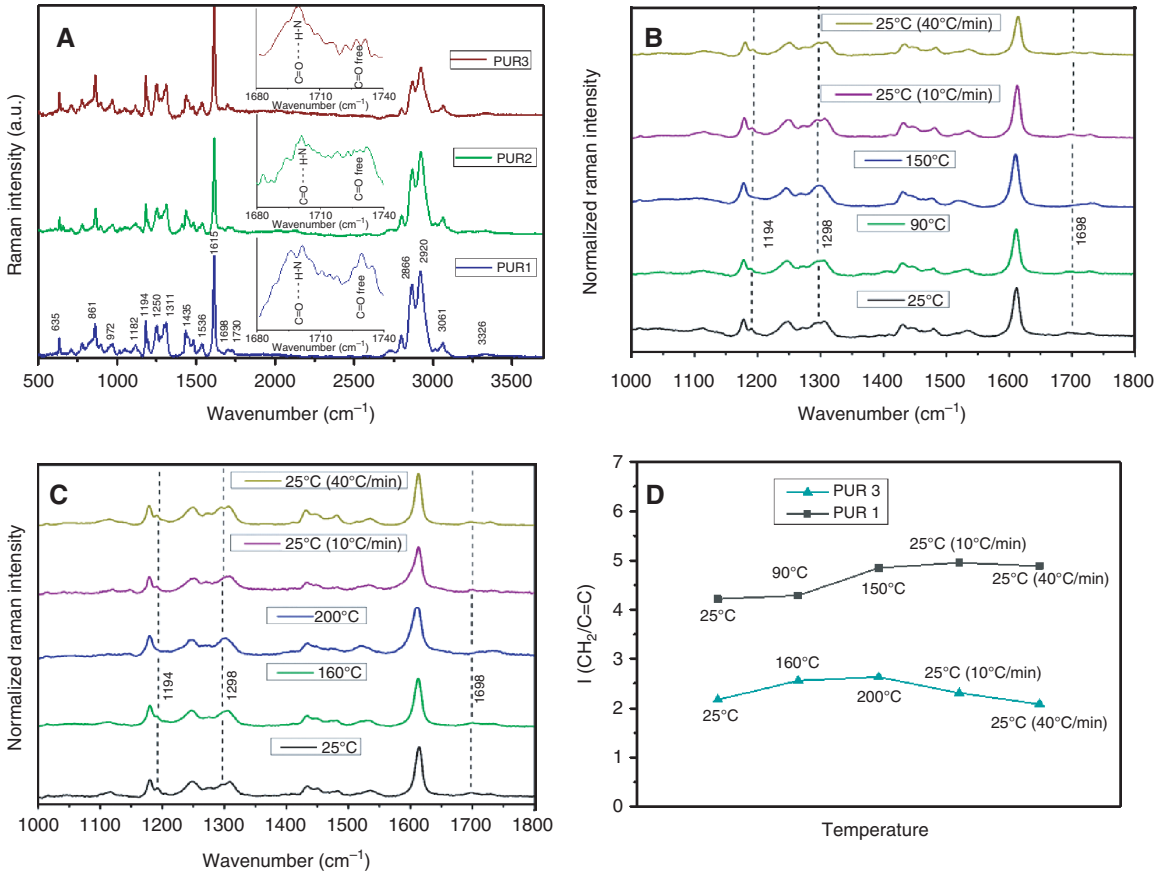

Figure 3: (A) Micro-Raman spectroscopy results at room temperature, (B) and (C) micro-Raman spectroscopy results of PUR1 and PUR3 at different temperatures and (D) relative Raman intensities of CH_2/C=C groups at different temperatures.

and carbonyl groups due to the HS-HS interactions [24–26]. The band intensities at 1699 cm^{-1} indicate higher amount of hydrogen bonds in PUR3 sample and, in consequence, a higher ability to form HDs. This result is in agreement with DSC measurements.

In order to study the effect of the temperature on the morphology development, Raman spectroscopy experiments were also carried out with varying temperature (Figure 3B and C). The main results are associated to the slight decrease in the band intensities at 1193 cm^{-1}, 1298 cm^{-1} and 1699 cm^{-1}. These signals disappeared at 200°C, but they reappeared after cooling.

The band at 1699 cm^{-1} is related to HS-HS interactions by hydrogen bonds [27]. The measurements indicated progressive disruption of the HDS with the increase of temperature. Similar behavior was observed for PUR3. From Figure 3C and D the relative intensities of CH_2 modes (2868 and 2925 cm^{-1}) relative to the aromatic ring mode C=C at 1615 cm^{-1} were calculated (Figure 4D). It can be noticed that relative intensities of CH_2 modes, compared with the aromatic ring mode, are higher for PUR1 (almost twice), confirming the higher concentration of flexible domains and aliphatic chains in PUR1. Also, it can be observed that the relative intensities of PUR2 increase with the temperature indicating changes of the structures due to the progressive decrease of the HDs (related to C=C groups) by melting. Note that when PUR3 sample was cooled at 40°C/min the curve gets a lower value than the initial value (also lower than at 10°C/min), indicating that the lower cooling stimulates HD formation. PUR1 sample slightly followed the same behavior at 40°C/min, but the HS did not equal the content at room temperature.

In order to support the last statement and because the final morphology should be mainly dominated by the structure formed in the melt state, AFM images were taken.

3.4 AFM and morphology development

Figure 4 shows the AFM images for the PURs. Brighter zones mean more mechanical dissipation as the tip taps on the sample and therefore corresponds to the SSs, while darker zones correspond to HSs [11, 28].

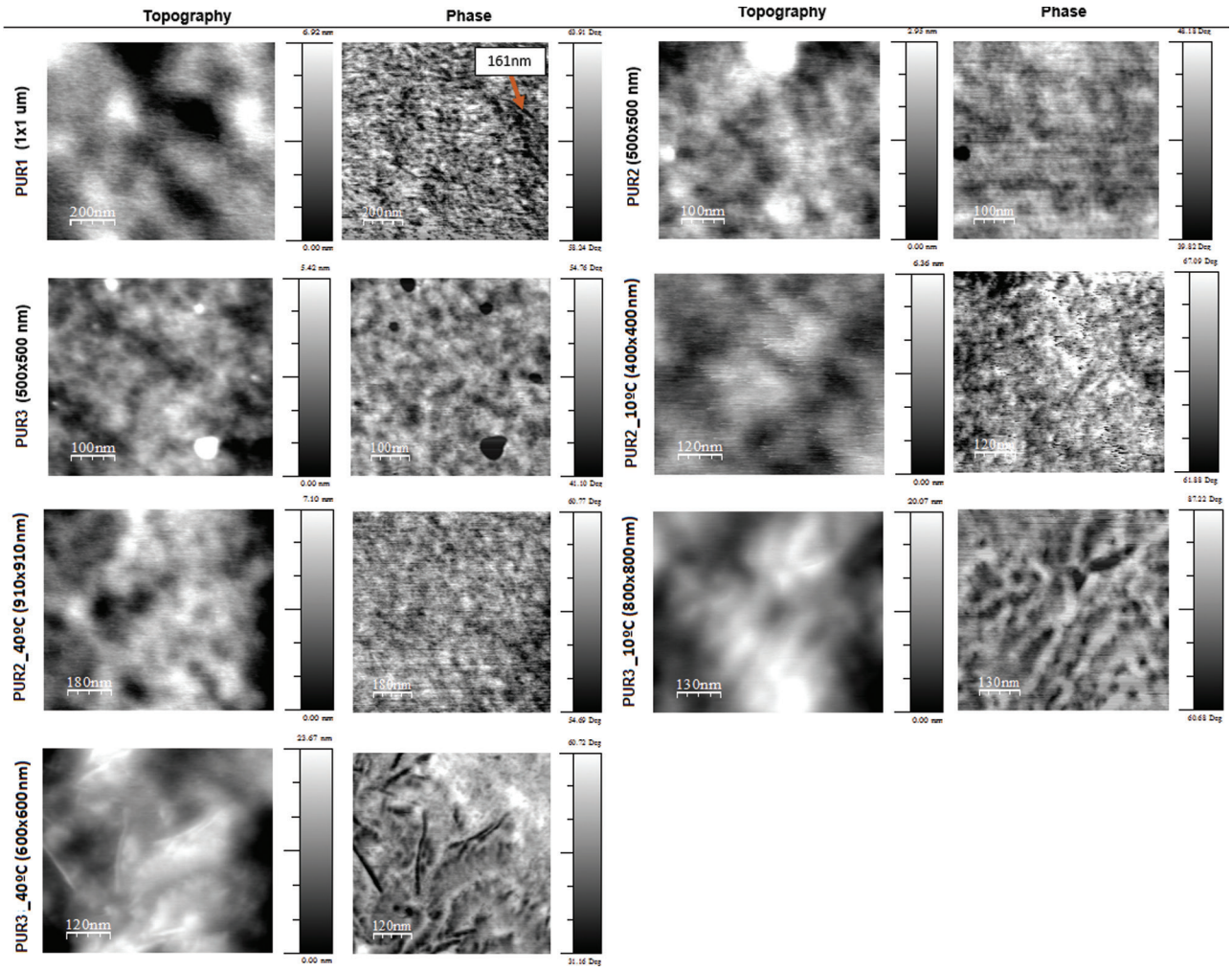

Figure 4: Topography and phase images of PURs. Note: an arrow denotes a hard domain.

In relation with the phase segregation suggested in the DSC results, small and well-distributed HDs could be formed in the PUR1 sample, ranging from 7 nm (circular) to 161 nm (elongated domains). The HDs of PUR2 went from 9 nm, and in general all have circular shape of approximately 39 nm. For PUR3 more defined HDs could be observed ranging from 10 nm to 45 nm. The samples were also heated until 200°C and remained for 5 min at that temperature, followed by a controlled cooling ramp at 10°C/min and 40°C/min, just like the program for the DSC. After cooling PUR1, it was not possible to identify a phase contrast; therefore, these results are not shown. Nevertheless, for PUR2 and PUR3, the morphology was very affected by the cooling rate. Both samples showed larger HDs after cooling at 10°C/min. At 40°C/min the morphology of PUR3 presented some HDs in the form of elongated domains; it seems that the higher content of HSs tend to form HDs.

From the previous characterization results, a scheme for the morphology development is proposed below. The schematic representation of the morphology development is presented in Figure 5. PUR3 with higher HS content could form larger HDs for cooling at both 10°C/min and 40°C/min. Compared to PUR3, samples with lower HSs (PUR1 and PUR2) were not able to achieve larger HDs even at low cooling rates.

3.5 Thermal stability (TGA)

Figure 6 shows the thermograms obtained by TGA in inert atmosphere for the samples. The weight loss is presented in Figure 6A and the corresponding derivative thermograms (DTG) in Figure 6B. For all samples three degradation processes are observed in a range of temperatures between 270°C and 550°C. No water absorption was seen for PUR1 and PUR2.

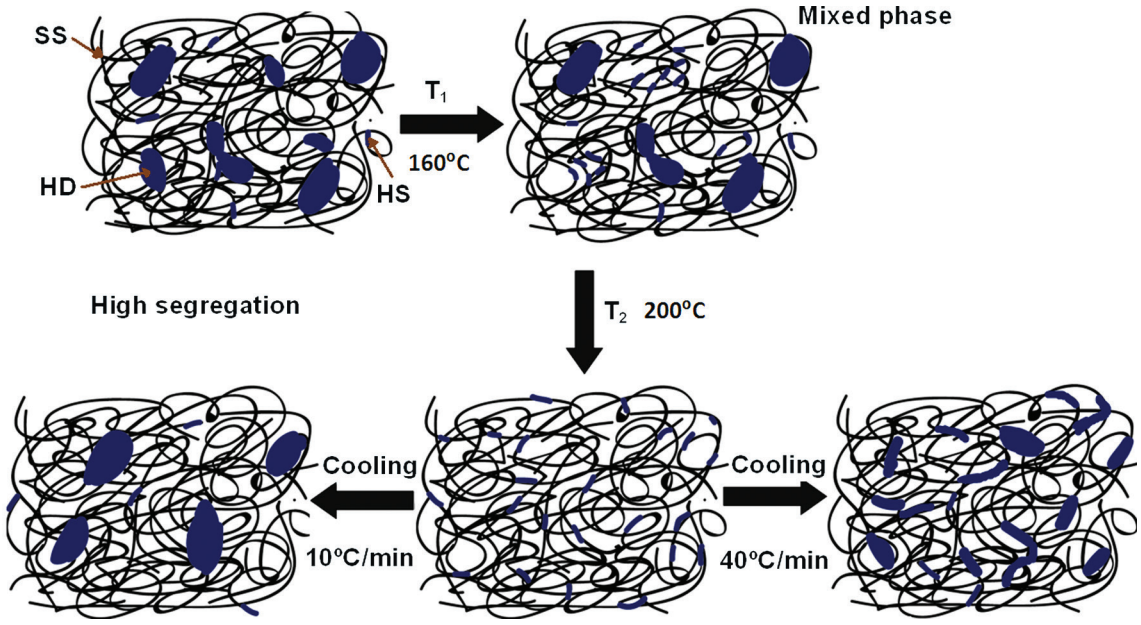

Figure 5: Morphology development induced by controlled cooling crystallization of PURs.

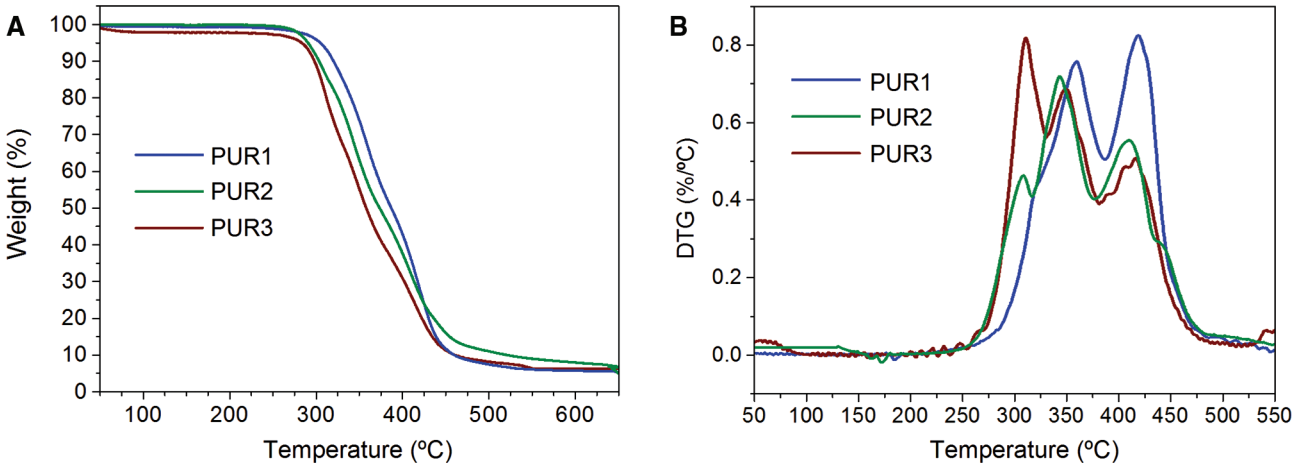

Figure 6: (A) TG curves under nitrogen and (B) DTG curves.

Three pathways for the cleavage of the PURs are known. One of them is the dissociation to isocyanate and alcohol. The other is the dissociation to primary amine, olefin, and carbon dioxide, and finally, the third process is the elimination of carbon dioxide, leading to formation of a secondary amine [29, 30]. Herrera et al. [31] reported that the first degradation process corresponds to the dissociation of urethane bonds, releasing primary amine, olefin, and carbon dioxide. In the second degradation process, water, HCN, or some nitriles and 1,4-BD or oligomers are produced from the chain extender and PTMG. Finally, the last degradation process corresponds to the decomposition of the char formed.

An initial weight loss of 29% can be observed at 311°C for PUR3 sample, 15% for PUR2, and 9% for PUR1 (represented by a small shoulder in the DTG curve at 319°C). This result can be associated to the higher MDI content of PUR3 and the higher thermal stability of the C-C bond with respect to NH-C(=O)-O group. The second degradation process is associated to the decomposition of the PTMG, and it was higher for PUR1. Finally, the last process corresponds to 31% and 44% of char products for PUR1 and PUR2, respectively. The last weight loss is higher for PUR1 due to lower MDI content, because of the loss of volatiles and byproducts formed after thermal degradation in the first decomposition step.

3.6 Mechanical properties

Shore A hardness measurements were carried out according to the ASTM D-2240 test method [32] (Figure 7A), while the elastic modulus obtained by nanoindentation is shown in Figure 7B.

Values of 70.1 for PUR1, 76.0 for PUR2, and 89.2 for PUR3 in the Shore A scale were obtained. As expected, when increasing the HS content, the materials became more rigid and hardness increased. These values are typically obtained for thermoplastic PURs and natural rubber. Nanoindentation results are more sensitive to changes in the structure of the materials and showed this similar trend. Average elastic moduli were 16.5 MPa, 19.2 MPa, and 71.0 MPa for PUR1, PUR2, and PUR3, respectively. These results remark the high influence of the HS content upon the mechanical properties of the materials.

3.7 Rheological measurements

In order to verify the thermal transitions previously assigned, rheological experiments were made at two different temperatures based on the DSC results. For PUR1, 190°C (in the second endothermic peak) and 200°C (completely molten) were chosen. Similarly for PUR1, the measurements were made at 150°C and 160°C.

Figure 8A represents the shear viscosity results plotted against the shear rate for both PUR1 and PUR3 samples. Note that even though the measurements for PUR3 were made at higher temperatures; in general its viscosity was higher due to the high HS content and its stronger structure. Nevertheless, PUR3 showed more dependence on the shear rate; this behavior is very common in polymers with high molecular weight. At 190°C PUR3 initially showed a shear thickening behavior and then, at 0.001 s^{-1} shifted to

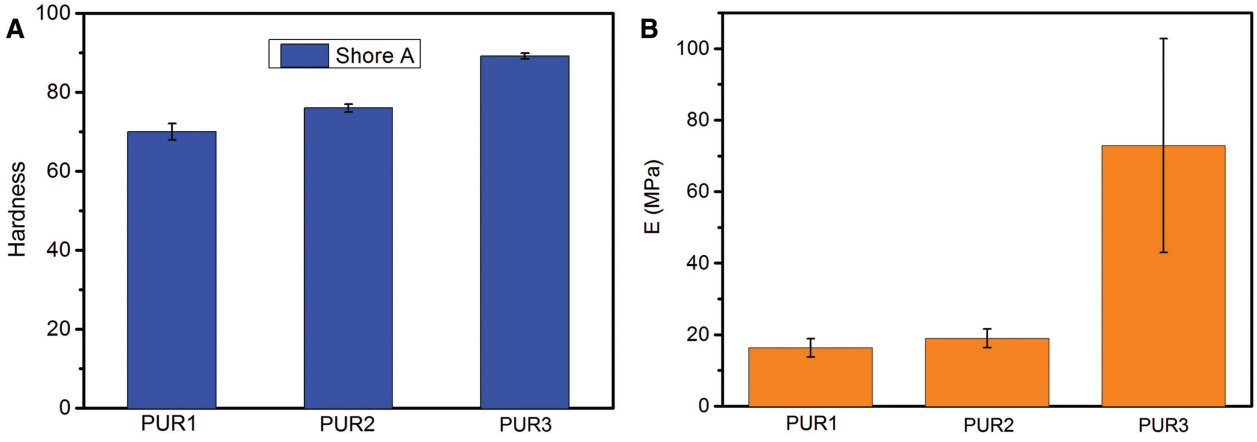

Figure 7: (A) Shore A hardness and (B) elastic modulus of the thermoplastic polyurethane samples.

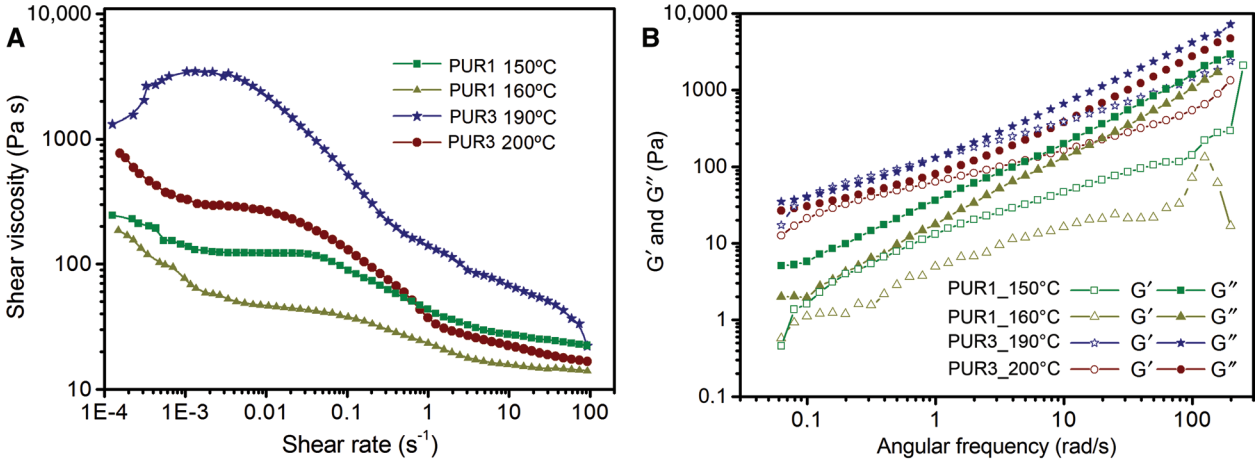

Figure 8: (A) Shear viscosity versus shear rate for PURs at two different temperatures; (B) elastic (G′) and loss modulus (G″) for PURs at two different temperatures.

shear thinning. This is probably because the temperature (190°C) is too close to the HDs melting temperature and in that condition some domains are not melted; melting domains can re-crystallize [33]. At 200°C PUR3 was completely molten, and the increasing shear rate caused a viscosity drop, but after shear values of 0.001 s^{-1} a little Newtonian plateau could be observed, indicating some kind of stability, due to the copolymeric nature of the material.

For PUR1 sample, both temperatures showed a behavior similar to that of PUR3 at 200°C, indicating that the material is totally melted at 150°C. Also, a Newtonian plateau was observed in the same shear rate regions. For shear values >0.6 s^{-1} PUR3 viscosity at 200°C is lower than PUR2 at 150°C.

Higher moduli were obtained for PUR3 sample, and it was found that for 190°C at low frequencies there is a modulus shift, confirming the re-crystallization of some HDs, in concordance with viscometry results. Later, at about 1.2 rad/s the viscous modulus predominates. For the other measurements a crossover point ($G' = G''$) was not found, and the viscous modulus predominated over the elastic during the complete angular frequency sweep. In general, the frequency increment caused the gap between G′ and G″ to become larger, favoring the viscous behavior at higher frequencies. This can be an advantage, because less energy could be required for their processing and complex shapes could be obtained by injection molding.

4 Conclusions

The synthesis and characterization of three segmented PURs prepared by a two-step solution polymerization were studied. Specifically, the influence of HSs on the crystallization was induced by both structure and controlled cooling. HDs formation and the phase separation were very dependent on the HS content. TGA results showed that all samples were thermally stable until 230°C. According to the DSC analysis, large presence of HS in the structure allows the development of more crystalline HDs, and this crystallization process is highly dependent on the cooling rate. Raman spectra demonstrated the HDs rupture at 150°C and 200°C for PUR1 and PUR3, respectively, and their subsequent controlled re-crystallization after cooling, which led to the proposal of a scheme of the morphology after controlled crystallization, in which high contents of HSs and low cooling rates enhance the crystallinity of the materials and change the mechanical properties as also the rheological behavior of the copolymer.

Acknowledgments: The authors would like to thank the program "Estrategia de Sostenibilidad 2015–2016, Universidad de Antioquia". We also want to thank "Colciencias movilidad Colombia-Argentina 533, 2011". Finally, the support of Prof. Arvind Raman and Maria José Cadena from Purdue University with the AFM measurements, Prof. Juan Meza with the nanoindentation measurements, and Adriana Valencia with the Raman measurements are greatly appreciated.

References

[1] Marín Bernabé, R. In Departament d'Enginyeria Química, Universitat Politècnica de Catalunya: Catalunya, 2009, Vol. Ph.D. Thesis, pp 253.
[2] Baudis S, Ligon SC, Seidler K, Weigel G, Grasl C, Bergmeister H, Schima H, Liska R. *J. Polym. Sci. Polym. Chem*. 2012, 50, 1272–1280.
[3] Bistričić L, Baranović G, Leskovac M, Bajsić EG. *Eur. Polym. J*. 2010, 46, 1975–1987.
[4] Kiran S, James NR, Jayakrishnan A, Joseph R. *J. Biomed. Mater. Res.-A* 2012, 100 A, 3472–3479.
[5] Pizzatto L, Lizot A, Fiorio R, Amorim CL, Machado G, Giovanela M, Zattera AJ, Crespo JS. *Mater. Sci. Eng. C* 2009, 29, 474–478.
[6] González-Paz RJ, Ferreira AM, Mattu C, Boccafoschi F, Lligadas G, Ronda JC, Galià M, Cádiz V, Ciardelli G. *React. Funct. Polym.* 2013, 73, 690–697.
[7] Chen Q, Liang S, Thouas GA. *Prog. Polym. Sci*. 2013, 38, 584–671.
[8] Guan J, Sacks MS, Beckman EJ, Wagner WR. *Biomaterials* 2004, 25, 85–96.
[9] El-Fattah MA, El Saeed AM, Dardir MM, El-Sockary MA. *Prog. Org. Coat*. 2015, 89, 212–219.
[10] Zhang P, Tian S, Fan H, Chen Y, Yan J. *Prog. Org. Coat*. 2015, 89, 170–180.
[11] McLean RS, Sauer BB. *Macromolecules* 1997, 30, 8314–8317.
[12] Velankar S, Cooper SL. *Macromolecules* 1998, 31, 9181–9192.
[13] Yang B, Huang WM, Li C, Li L, Chor JH. *Scripta Mater*. 2005, 53, 105–107.
[14] Crawford DM, Bass RG, Haas TW. *Thermochim. Acta* 1998, 323, 53–63.
[15] Lu G, Kalyon DM, Yilgör I, Yilgör E. *Polym. Eng. Sci*. 2003, 43, 1863–1877.
[16] Yoon PJ, Han CD. *Macromolecules* 2000, 33, 2171–2183.
[17] Hernandez R, Weksler J, Padsalgikar A, Taeyi C, Angelo E, Lin JS, Xu LC, Siedlecki CA, Runt J. *Macromolecules* 2008, 41, 9767–9776.
[18] Castagna AM, Fragiadakis D, Lee H, Choi T, Runt J. *Macromolecules* 2011, 44, 7831–7836.
[19] Aurilia M, Piscitelli F, Sorrentino L, Lavorgna M, Iannace S. *Eur. Polym. J*. 2011, 47, 925–936.

[20] Leung LM, Koberstein JT. *Macromolecules* 1986, 19, 706–713.
[21] Bagdi K, Molnár K, Kállay M, Schön P, Vancsó JG, Pukánszky B. *Eur. Polym. J.* 2012, 48, 1854–1865.
[22] Nichetti D, Grizzuti N. *Polym. Eng. Sci.* 2004, 54, 1514–1521.
[23] Janik H, Pałys B, Petrovic ZS. *Macromol. Rapid Comm.* 2003, 24, 265–268.
[24] Roohpour N, Wasikiewicz J, Paul D, Vadgama P, Rehman I. *J. Mater. Sci.-Mater. M.* 2009, 20, 1803–1814.
[25] Parnell S, Min K, Cakmak M. *Polymer* 2003, 44, 5137–5144.
[26] Cuéllar A, Mesa F, Vargas C, Perilla J. *Rev. Fac. Ing. Univ. Ant.* 2010, 54, 57–64.
[27] El-Abassy RM, Donfack P, Materny A. *Food Res. Int.* 2010, 43, 694–700.
[28] Yanagihara Y, Osaka N, Murayama S, Saito H. *Polymer* 2013, 54, 2183–2189.
[29] Yoshitake N, Furukawa M. *J. Anal. Appl. Pyrol.* 1995, 33, 269–281.
[30] Lattimer RP, Polce MJ, Wesdemiotis C. *J. Anal. Appl. Pyrol.* 1998, 48, 1–15.
[31] Herrera M, Matuschek G, Kettrup A. *Polym. Degrad. Stabil.* 2002, 78, 323–331.
[32] ASTM. West Conshohocken, PA 19428-2959. United States, 2010.
[33] Yamasaki S, Nishiguchi D, Kojio K, Furukawa M. *Polymer* 2007, 48, 4793–4803.